Macromolecules

pubs.acs.org/Macromolecules Article

Organic *Versus* Inorganic Supports for Metallocenes: The Influence of Rigidity on the Homogeneity of the Polyolefin Microstructure and Properties

Zahra-Alsadat Hejazi-Dehaghani, Hassan Arabi,* Daniel Thalheim, Danijel Vidakovic, Mehdi Nekoomanesh Haghighi, Lothar Veith, and Markus Klapper*

Cite This: *Macromolecules* 2021, 54, 2667−2680 Read Online

ACCESS | Metrics & More | Article Recommendations | Supporting Information

ABSTRACT: A procedure to obtain very uniform polyolefin copolymers by supported metallocenes is presented. Conventional metallocene or Ziegler−Natta catalysts, both immobilized on inorganic supports, yield only copolymers with inhomogeneous comonomer incorporation and broad short-chain branching distribution. The main reasons are diffusional limitations of the monomers or the multisite character of the catalysts. By comparing inorganic and organic supports, we demonstrate that metallocenes immobilized on organic supports solve these problems. In this regard, organic and soft nanosized polystyrene particles (nPS) *versus* industrially used, hard, and inorganic SiO_2 were used to support [$Me_2Si(Ind)_2ZrCl_2$/MAO (**I**) and $Me_2Si(Benz[e]\text{-}Ind)_2ZrCl_2$/MAO (**BI**)] catalysts for ethylene/1-hexene copolymerization. In the inorganic case, the catalyst systems show a substantial inconsistency in the copolymers' branching distribution, resulting in phase separation. One phase is hexene-poor with high melting temperature (T_m) and high molecular weight (MW). The second, hexene-rich phase, however, shows lower T_m and MW. By using organic supports, comonomers are uniformly inserted into the polymer chain and homogeneous microstructured copolymers are obtained. These findings are mainly attributed to diffusion processes of the monomers into the soft organic material. To prove this conclusion and to elucidate the structure of the catalyst system, various characterization techniques such as time-of-flight secondary ion mass spectrometry and scanning electron microscopy−energy-dispersive X-ray were performed.

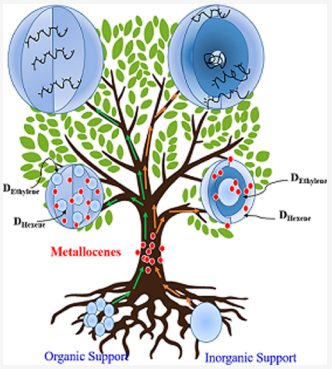

1. INTRODUCTION

The copolymerization of ethylene with α-olefins has resulted in a growth of polyolefin applications over the last decades.[1,2] In particular, metallocene-catalyzed copolymerization represents a versatile synthetic route to tailor-made polyolefins.[1,3,4] In comparison to Ziegler−Natta catalysts, metallocenes have shown remarkable advantages, such as regulating the polymer microstructure by narrow molecular weight (MW) distribution and stereoselective comonomer incorporation.[5−9] Nevertheless, homogenous metallocene catalysts cause reactor leaching/fouling because of a lack of morphology control during polymerization.[10] Therefore, metallocenes have been supported on micrometer-sized fragmentable porous particles. The use of such catalyst systems has enabled their application in a wide range of industrial processes,[11−13] with the advantage of the dramatic reduction in the necessary amount of methylaluminoxane (MAO).[14,15]

The ability of the microsized support (10−100 μm) to fragments is a prerequisite necessity for an applicable catalyst system; subsequently, fragmentation down to the nanometer scale (20−200 nm) guarantees to obtain high activity and transparent products because small enough fragments do not scatter light.[5,10] Furthermore, a replication effect determines the morphology, like the size and shape, which is decisive to gain a flowable product with a high bulk density.[11,16,17] Complete fragmentation of supports has sometimes been challenging to attain and has troubled the commercialization of polyolefins based on metallocenes.[18]

Two main fragmentation models, that is, multigrain and layer-by-layer, are established and developed so far by scanning electron microscopy (SEM), transmission electron microscopy, and laser scanning confocal fluorescence microscopy (LSCFM).[10,18−20] For example, $MgCl_2$ used for Ziegler−Natta catalysts undergoes multigrain polymerization, where fragmentation occurs from the onset of the polymerization throughout the whole particle simultaneously. However, silica supports follow a gradually layer-by-layer fragmentation model. In this case, the silica-supported catalysts fragment from the outside to the core (layer-by-layer) by the polyolefin particle growth. Mass-transfer resistance hinders this fragmentation

Received: August 19, 2020
Revised: January 12, 2021
Published: February 1, 2021

https://dx.doi.org/10.1021/acs.macromol.0c01920
Macromolecules 2021, 54, 2667−2680

behavior during the polymerization process, caused by slowing down the intraparticle diffusion of the monomers into the pores.[10]

The mass transfer resistance becomes even more complicated when α-olefins as comonomers were introduced in the polymerization. Fink et al. elucidated the inconsistency in the chemical composition distribution (CCD) of the copolymer particles by SEM and called it the "filter-effect".[21] Accordingly, McKenna and Ahsan Bashir reported the direct correlation between physical properties of the silica support (i.e., particle size and porosity) and mass-transfer resistance in the initial instants of the (co)polymerization.[16] This intraparticle monomer diffusion resistance dependency on the catalyst particle size is higher in larger catalyst particles during the first stage of ethylene polymerization.

It should be noted that the origin of this heterogeneity in the copolymers' CCD using silica-supported metallocenes is not comparable to those prepared with Ziegler−Natta systems. Metallocenes are single-site catalysts; this feature is almost independent of the interactions with the cocatalyst (except activity) or the surface of the support. In contrast, Ziegler−Natta catalysts are naturally multisite systems in which the number of active centers can vary by changes in the polymerization components and $MgCl_2$ surface structure. For example, Paulik et al. established for metallocene a narrow and for Ziegler−Natta catalysts a broad interchain distribution of 1-octene units in ethylene/1-octene copolymers.[8]

These remarks show a necessity to develop a catalyst system that allows the synthesis of very homogeneous microstructured copolymers. Therefore, it is essential to establish a system based on a single-site catalyst with uniform diffusion of all different monomers to the catalytic centers everywhere inside the support.

Herein, we assume that the organic-based support offers the chance to overcome this CCD inconsistency. In the previous publications, we have already demonstrated that organic supports, such as aggregates of nanosized polystyrene particles (nPS), show in ethylene or propylene polymerizations activity comparable to silica-based supports. Crucial supporting requirements by versatile functionalization of the support surface,[22] fragment ability, and high activity[23,24] are fulfilled. The use of suitable emulsifiers [Lutensol A50, which stays on the particle surfaces as a polyethylene glycol (PEG) chain] allows for tailoring the surface nucleophilicity to ensure MAO or catalyst immobilization.[10]

The nanosized primary particles reversibly agglomerate and form secondary particles in the presence of MAO with a size of few microns.[14] Because MAO and nucleophilic groups are noncovalently bonded, the secondary particles fragment friably by hydraulic forces of the polymer propagation between nPS particles. The main difference in polymerization processes using inorganic supports is the swelling of the secondary clusters with monomers or media and diffusion behavior of the "soft organic support," as the monomers can more easily be uptaken and move thoroughly. We have already proven this for ethylene homopolymerizations by fragmentation studies via LSCFM.[10,18] The LSCFM studies of the polymer growth with time showed a nifty multigrain fragmentation process for the aggregates of the nPS-supported catalyst particles (opposite of silica with a layer-by-layer fragmentation).

In this study, the influence of the support nature/type on the comonomer incorporation is at the center of the investigation to find a way to solve the challenge of producing copolymers with a homogenous composition by a supported metallocene. Organic nPS particles are studied for the immobilization of metallocene catalysts in copolymerization processes compared to silica as an inorganic support. Two different silylene-bridged bis(indenyl) catalysts are chosen, which are reported as highly active to incorporate the comonomer in homogenous catalyst systems (solution polymerization).[25]

2. EXPERIMENTAL SECTION

All oxygen- and moisture-sensitive experiments are performed under an inert atmosphere using standard Schlenk and glovebox techniques.

2.1. Chemicals. Silicon dioxide (SiO_2), chemically prepared with an average diameter of 50 μm and a surface area of 500 $m^2\ g^{-1}$, was procured from Degussa AG under the trade name Sipernat 50. $Me_2Si(Ind)_2ZrCl_2$ (**I**) and $Me_2Si(Benz[e]\text{-}Ind)_2ZrCl_2$ (**BI**) were purchased from MCAT GmbH. Modified MAO (MMAO) (10 wt % solution in toluene), triisobutyl aluminum (TiBAl, 1 M solution in hexane), and highly pure heptane (99.99%) were obtained from Sigma-Aldrich and used as received. Dry toluene and 1-hexene were additionally distilled over sodium metal and stored over molecular sieves in the glovebox. Ethylene (Linde AG) was purified by passing through Supelco deoxygenation and moisture trap columns.

2.2. Support Preparation. Nanopolystyrene PEO-functionalized particles (nPS) and SiO_2 supports were prepared as described.[22]

2.3. Nanopolystyrene Particles. Lutensol AT50 (400 mg, 0.16 mmol) and cetyl trimethyl ammonium bromide (22 mg, 0.06 mmol) were dissolved in distilled water (100 mL) at 40 °C and stirred for 30 min. Styrene (5 g, 48.0 mmol), divinylbenzene (0.91 g, 7.0 mmol), and hexadecane(0.42 g, 1.86 mmol) as nonaqueous parts were mixed and added to the water/emulsifier mixture at room temperature. The solution was agitated for 30 min and then sonicated with a Branson Sonifier 450W, 70% power under ice-cooling for 7 min to form miniemulsion. The miniemulsion was degassed with argon for 20 min and then heated to 70 °C. The initiator for radical polymerization, azodiiso-butyramidinedihydrochloride (210 mg, 0.77 mmol), was dissolved in 10 mL of distilled water, degassed for 20 min, and added to the miniemulsion. After 12 h, the mixture was filtered and purified by forced dialysis with at least 300 mL of water and afterward frozen and lyophilized. After drying overnight under vacuum, particles were transferred to the glovebox. The size of the particles in a highly diluted suspension was determined via dynamic light scattering (Zetasizer) to be 40−60 nm.

2.4. SiO_2 Particles. Silica (2 g) was calcined at 400 °C under vacuum for 3−5 h to reach constant weight. Calcinated silica (1 g) was impregnated with 6 mL of MMAO in 8 mL of toluene stirred at 100 rpm for 2 h. The suspension was filtered and washed three times with 8 mL of toluene. The filter cake was dried under reduced pressure. The SiO_2−MAO particles (herein called "SiO_2") were stored in the glovebox.

2.5. Catalyst Preparation. *2.5.1. nPS Support Suspension.* The support (50 mg) was suspended in toluene (5 mL) with sonication to disperse primary particles efficiently. After dispersion, 1 mL of MMAO was added to the suspension to scavenge potential traces of impurities or accessible functional groups. The mixture was agitated for 2 h. The suspension was redispersed by sonification before adding an activated catalyst solution.

2.5.2. Silica Support Suspension. Before every catalyst synthesis, 50 mg of the ready SiO_2−MAO was dispersed in 5 mL of toluene and shaken for 2 h.

2.5.3. Catalyst Impregnation. After preparing the support suspension, the dissolved and preactivated solution of 5 mg of **BI** or **I** with 1.2 mL of MAO in 3 mL of toluene for 2 h was added to each of the support suspensions. To immobilize the catalyst, the mixture was agitated at 100 rpm for 2 h. After that, the supernatant catalyst solution was removed over a G4 glass frit and washed three times with 3 mL of toluene to remove any residual free catalyst. The remaining filter cake—the supported catalyst—was ready to use after drying under vacuum.

https://dx.doi.org/10.1021/acs.macromol.0c01920
Macromolecules 2021, 54, 2667−2680

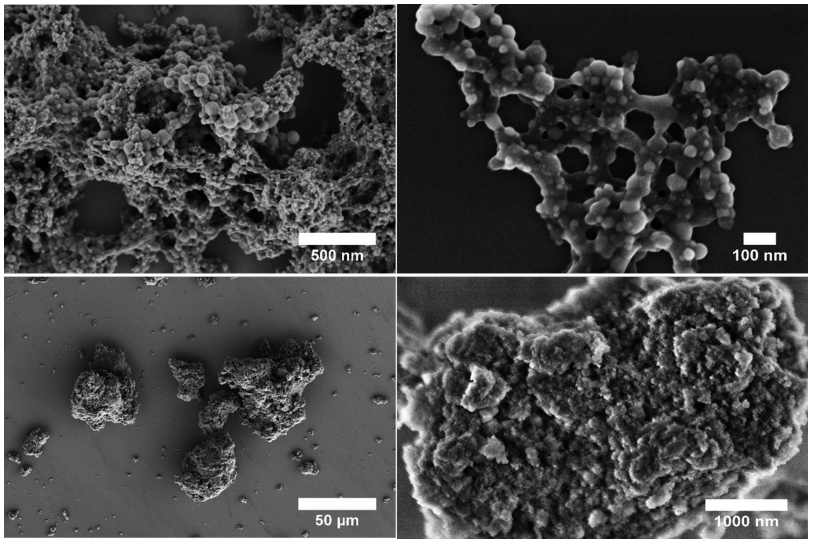

Figure 1. SEM images of the treated (top) nPS and (bottom) SiO_2 with MAO.

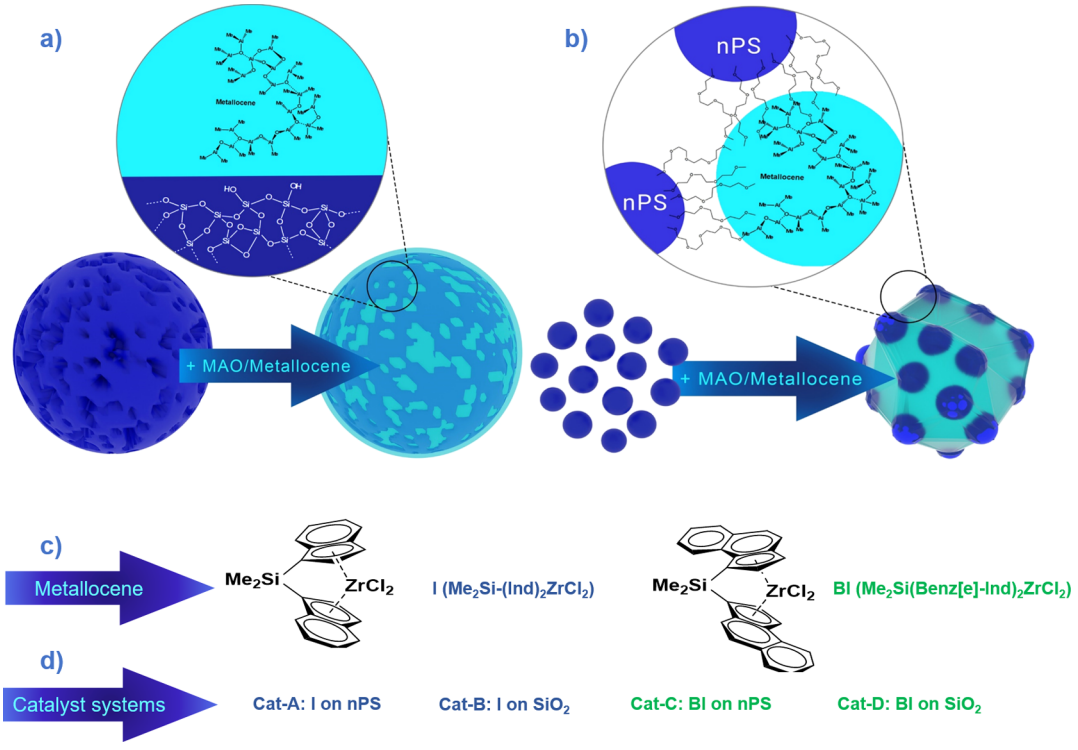

Figure 2. Scheme of catalyst immobilization process (a) on inorganic SiO_2−MAO and (b) on organic nPS−MAO supports, (c) metallocene structures, and (d) naming of the catalyst systems used in this study.

2.5.4. (Co)polymerization of Ethylene/1-Hexene. The (co)-polymerizations were conducted in a 250 mL glass reactor from Büchi Glas Uster AG at 60 °C and an ethylene overpressure of 3.0 bar. A glass centrifugal stirrer was used at 1500 rpm to stir the slurry mixture. The reactor was filled with a total volume of 100 mL of heptane, TiBAl (1 mL, as a scavenger), and comonomer (for copolymerization). The media were then saturated with ethylene for 20 min before injecting the catalyst (~10 mg of the supported catalyst) suspension into the reactor by argon overpressure. The ethylene pressure was kept constant by continuously monitoring and recording ethylene consumption with a mass flow controller and replacing it as it was consumed. Polymerization was stopped by releasing the ethylene pressure and quenching the catalyst by adding acidic methanol. The reaction mixture was stirred until the system cooled down to room temperature, filtered, and dried under vacuum.

2.5.5. Characterization. The chemical composition of catalysts was measured by inductively coupled plasma optical emission spectroscopy (ICP-OES, Jobin-Yvon Activa M). The aluminum distribution on the supports was characterized by ToF-SIMS (time-of-flight secondary ion mass spectrometry, IONTOF TOF.SIMS5 NCS) and SEM with energy-dispersive X-ray analysis (SEM−EDX, a Hitachi SU-8000 and Bruker). The aluminum diffusion depth was investigated by ToF-SIMS imaging (fast imaging mode) of the particle cross sections after cutting samples by a focused-ion beam instrument. The ^{13}C nuclear magnetic resonance (^{13}C NMR, Bruker 500 MHz NMR Spectrometer AVANCE) spectra of the homo- and copolymers were recorded from solutions of 40−50 mg of polymers in 0.5 mL of

https://dx.doi.org/10.1021/acs.macromol.0c01920
Macromolecules 2021, 54, 2667−2680

Table 1. Elemental Analysis for the Catalyst Systems by ICP-EOS

		calculated			observed result			
catalyst	catalyst type	wt % of Zr	wt % of Al	Al/Zr	wt % of Zr	wt % of Al	(μmol Zr g^{-1} cat)	Al/Zr
Cat-A	**I** on PS	0.90	65	230	0.19 (21%)	58 (89%)	20.8	500
Cat-B	**I** on SiO_2	0.90	65	230	0.58 (64%)	28 (43%)	54.5	120
Cat-C	**BI** on PS	0.95	70	250	0.31 (34%)	70 (100%)	34.0	800
Cat-D	**BI** on SiO_2	0.95	70	250	0.50 (56%)	37.5 (53%)	63.9	220

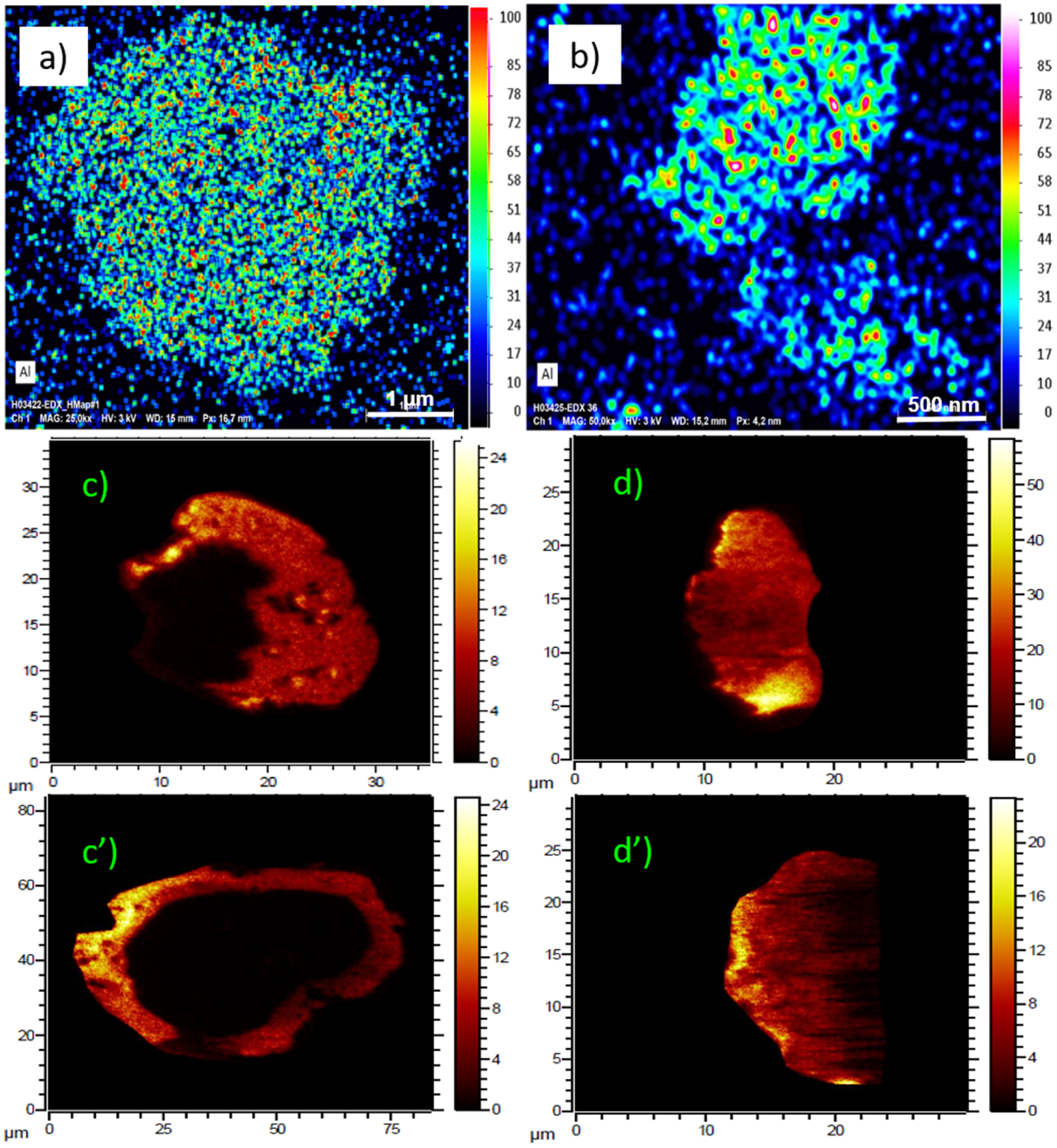

Figure 3. SEM−EDX of the Al mapping on (a) silica and (b) nPS. ToF-SIMS Al mapping of the cross-sectioned (c,c′) two silica particles and (d,d′) two nPS particles.

ODCB-d_4 at 135 °C with a 30° pulse angle (^{13}C NMR at 125 MHz, 10 s delay, and at least 4000 scans). The molar masses of the copolymers in 1,2,4-trichlorobenzene were determined with a high-temperature gel permeation chromatography instrument with an IR detector. The comonomer distribution depending on the MW was determined by using the internal calibration curve of the IR detector (see the Supporting Information, Figure S6). The melting endotherms were determined on a differential scanning calorimeter (DSC, Mettler Toledo DSC-823) in the temperature range of 20−200 °C using a heating rate of 10 °C min^{-1}. The heating cycle was performed twice, and the results of the second scan were reported. The crystallinity of the polymers was calculated by DSC and wide-angle X-ray diffraction

https://dx.doi.org/10.1021/acs.macromol.0c01920
Macromolecules 2021, 54, 2667−2680

Table 2. Activity of the Catalyst Systems in Homo- and Copolymerization of Ethylene (Polymerization Conditions: 100 mL of Scavenged Heptane, 3 Bar Ethylene Pressure, 60 °C, 20 min, ≈ 10 mg Supported Catalyst)

run	catalyst	sample	$C_{6\text{-feed}}$ (mmol L^{-1})	yield (g)	(μmol Zr g^{-1} cat)	activity (Kg PE mol^{-1} Zr h^{-1} bar^{-1})
1	Cat-A	PE-I-nPS	0	0.92	20.8	3000
2		PEH70-I-nPS	70	1.39		4600
3		PEH150-I-nPS	150	1.32		4200
4	Cat-B	PE-I-SiO_2	0	0.74	54.5	1600
5		PEH70-I-SiO_2	70	0.87		1700
6		PEH150-I-SiO_2	150	1.18		1900
7	Cat-C	PE-BI-nPS	0	0.91	34.0	3100
8		PEH70-BI-nPS	70	1.95		8260
9		PEH150-BI-nPS	150	1.64		5300
10	Cat-D	PE-BI-SiO_2	0	1.10	63.9	1650
11		PEH70-BI-SiO_2	70	2.70		4450
12		PEH150-BI-SiO_2	150	1.77		3300

(XRD, MicroMax 007 rotating anode). To calculate the crystallinity by XRD, Peakfit v4.12 was used to estimate the surface area under the peaks pertained to crystalline and amorphous parts (see the example in the Supporting Information, Figure S7). For the determination of the comonomer distribution variation, the successive self-nucleation annealing (SSA) technique was implemented. For the studies, all of the thermal fractionation steps were carried out at a thermal window of 5 °C, heating and cooling rates of 10°C min^{-1}, and 12 cycles of heating and cooling (see Supporting Information, Figure S9).

3. RESULTS AND DISCUSSION

To further investigate the influence of the support type (i.e., organic *vs* inorganic supports) on the comonomer incorporation behavior; $Me_2Si[Ind]_2ZrCl_2$/MAO (**I**) and $Me_2Si(Benz[e]\text{-}Ind)_2ZrCl_2$/MAO (**BI**) were loaded on silica and nPS particles. Before and after copolymerization, various characterization techniques were utilized to study the influence of the catalyst chemical composition on the polymerization behavior and polymer properties, first at the molecular and then at the macroscopic level properties.

3.1. Catalyst Loading on Organic and Inorganic Supports. For organic substrates, polystyrene nanoparticles (nPS) are introduced as "primary particles" with a size of 40−60 nm. Therefore, defined functionalities on the surface of nPS particles are crucial for controlling reversible self-assembly toward larger aggregates (secondary particles) in the micrometer range (1−100 μm—Figure 1) by the interaction of MAO and PEG chains of the nPS particles. Nanopolystyrene latex particles containing PEG chains, as a stabilizer, were prepared via miniemulsion polymerization.[5,22] Suitable stabilizers stay physically connected to the particles and allow noncovalent immobilization of active MAO/metallocene complexes (Figure 2b).[10] In ethylene (co)polymerization, these aggregated clusters fragmented down to primary latex particles to guarantee high activity and high bulk density.[19]

The organic nPS particles were applied as the catalyst support for the metallocene, yielding Cat-A (**I** on nPS) and Cat-C (**BI** on nPS). For comparison, both catalysts were immobilized on SiO_2−MAO using the same procedure (Figure 2a), which produced Cat-B (**I** on SiO_2) and Cat-D (**BI** on SiO_2).

ICP-OES elemental analysis of zirconium and aluminum (Table 1) of all four catalyst systems (Cat-A to Cat-D) showed that in the case of using the nPS support, 20−30 wt % of the added zirconium was adsorbed on the organic support, while it was 2−3 fold higher (55−65 wt %) for the inorganic support. A reverse trend was demonstrated for the absorbing/penetrating aluminum on both supports. In Cat-A and Cat-C, nearly all provided MAO during the synthesis was absorbed, but only half of the Al content was absorbed in the final catalyst for silica counterparts (Cat-B and Cat-D).

The different catalyst immobilization mechanisms explain the differences in the Al/Zr molar ratio on both supports. The catalyst deposition mostly occurs electrostatically by interactions between the activated catalyst species and the nucleophilic groups of the MAO support. Therefore, depending on the acidity of the functional groups on the supports, MAO and catalyst affinity can vary. The interactions between SiO_2/MAO/metallocenes are well established.[26] The SEM images of both treated supports with MAO are presented in Figure 1. These images show how nPS supports self-assembly and produces clusters with MAO for trapping metallocenes. The activated catalyst species intercalate in the formed nPS−MAO cages by electrostatic interactions. Both catalysts, **I** and **BI**, can diffuse sufficiently into the MAO cage. Thus, nonadsorbed/nonimpregnated activated catalysts were filtered off along with the solvent during catalyst washings.

As metallocenes can form active centers wherever aluminum compounds are present, the aluminum distribution was investigated using SEM−EDX after treating both support types with MAO. The resulting images with shading colors correlated to the intensity of the element present (Figure 3a,b) demonstrate that Al is evenly distributed on the surface of both supports. To explain the differences in the Al/Zr molar ratios for both supports, additionally, cross-sectioned particles (using a focused ion beam) of each support were studied by ToF-SIMS. The results illustrated heterogeneous and homogeneous Al distributions for SiO_2 and nPS supports (Figure 3c,c′, d,d′), respectively. Aluminum is distributed uniformly on the surface and inside of the nPS secondary particles. In this case, MAO acted as a glue and formed a larger cluster of nPS−MAO. The metallocenes were diffused inside the formed clusters, and only unbounded metallocene species are washed off. In contrast, it suggests that for the SiO_2 support used herein, the Al content decreases drastically from the outside of the particle toward the center. It indicates that for the SiO_2 supports, aluminum and therefore active center formation predominantly occurs close to the particle surfaces. As a result, after surface saturation, the excess/free MAO and metallocenes are washed off.

3.2. Polymerization Kinetics and Activity of the Catalysts. The overall activity of a catalyst system is associated with catalyst activation−deactivation, comonomer effect, and fragmentation.[27,28] These properties depend on the

https://dx.doi.org/10.1021/acs.macromol.0c01920
Macromolecules 2021, 54, 2667−2680

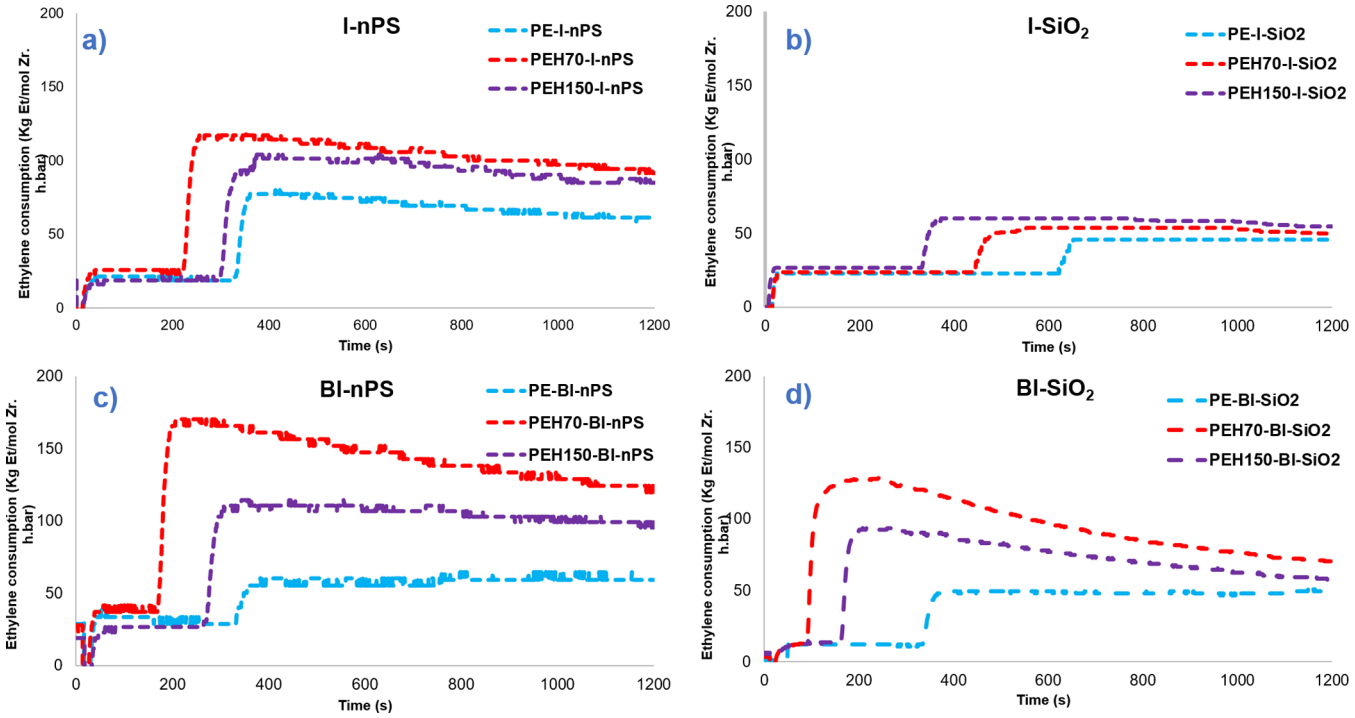

Figure 4. Kinetic behavior of A–D Metallocene catalysts: (a) Cat-A, (b) Cat-B, (c) Cat-C, and (d) Cat-D.

catalyst ligand structure and the support characteristics, for example, type, size, and size distribution of the support particles, which influenced the Al/Zr molar ratio. Moreover, supported catalysts may lead to a different geometry of active centers,[8] which, because of the surface of the support's geometry, retards catalyst behavior in regulating the monomer sequences. To elucidate the influence of these factors on the polymerization process, the kinetics were monitored by measuring ethylene consumption in performing polymerizations in heptane using catalyst systems Cat-A to Cat-D at 60 °C and an ethylene overpressure of 3 bar. (See Table 2; samples are named as PE(HX)-**I**-Y, where X stands for 1-hexene concentration and Y refers to the support type).

Using the polymer yield and Zr content (in Table 1), the activity of all catalyst systems in homo- and copolymerization of ethylene and 1-hexene is observed. In ethylene homopolymerizations, a comparison of the nPS- and silica-supported catalysts (Table 2) demonstrates that organic supports result in higher activity. For instance, Cat-A (3000 Kg PE mol^{-1} Zr h^{-1} bar^{-1} in run 1) and Cat-C (3100 Kg PE mol^{-1} Zr h^{-1} bar^{-1} in run 7) provided considerably higher activities than Cat-B (600 Kg PE mol^{-1} Zr h^{-1} bar^{-1}in run 4) and Cat-D (650 Kg PE mol^{-1} Zr h^{-1} bar^{-1} in run 11), respectively, under identical metallocene structure and polymerization conditions. It is attributed to the fact that polymeric supports fragment through a multigrain pathway.[18] During polymerization, the aggregated clusters (Figure 1) are entirely fragmented into the initial nanometer-sized particles (primary particles) within the final product because of the mechanical stress from the growth of polyolefins between the nPS particles. This fragmentation is possible because of the weaker cohesive forces of the secondary particles. Additionally, solvents and monomers partially swell the polymeric support cluster, accommodating monomer insertion and enabling access to the catalyst active centers. Because the formation of the active center of the catalyst depends on the presence of aluminum, according to the results of ToF-SIMS Al mapping (Figure 3d,d′ *vs* 3c,c′), it is interpreted that loading of catalysts on organic supports enabled a more uniform distribution of the active sites from the inner side to the outermost part of the particle, whereas the active sites of the catalyst on the silica support are mostly on the surface of the support.

In the presence of 1-hexene, ethylene consumption of all four catalyst systems, Cat-A to Cat-D, increased. In detail, catalyst activity for Cat-A and Cat-C increases from 3000 to 4600 (runs 1–3) and from 3100 to 8260 Kg PE mol^{-1} Zr h^{-1} bar^{-1} (runs 7–9), respectively. For silica-supported metallocenes, Cat-B and Cat-D, their corresponding activity was boosted from 1600 to 1900 (runs 4–6) and from 1650 to 4450 Kg PE mol^{-1} Zr h^{-1} bar^{-1} (runs 10–12), respectively. The referred positive "comonomer effect" (Figure 4) for metallocenes has been well studied by McDaniel et al.[29,30] The authors demonstrated that ethylene insertion is accelerated with the first small additions of comonomers (probably the coordination), which is a better electron donor than ethylene. They established that 1-hexene in the reactor could improve overall activity by up to 5–10 fold; however, the incorporation selectivity remained first order. This observation indicates that the incorporation rate of both monomers was similarly affected without having a substantial effect on the polymer properties.[29] The authors discussed various potential mechanisms for the comonomer effect, such as mass transfer effects, better electron donation of the comonomer with respect to ethylene, and reactivation of the dormant active centers.

In addition to the influence of the type of supports, catalyst **BI** responds better to the comonomer, and the polymerization rate increases more under identical conditions.

3.3. Structure–Property Relationship. Gaining insights into the behavior of the catalyst and the influence of the support is only possible by observing the characteristics of the polymer produced. Evidently, with given catalysts, the polymerization conditions, such as temperature, pressure, and

https://dx.doi.org/10.1021/acs.macromol.0c01920
Macromolecules 2021, 54, 2667–2680

more critically, type of support, regulate the final polymer structure. Thus, the behavior of the catalyst controls MW, MW distribution (MWD), short-chain branching content (SCB), and SCB distribution (SCBD). To explore the correlation between the type of the support and the polymer microstructure, polymer properties were studied using different characterization methods.

3.3.1. Molecular Weight and Molecular Weight Distribution. Indeed, for each catalyst system, Cat-A to Cat-D, the type of support is pivotally responsible for controlling MW and MWD, as shown in Table 3. The values show that the average

Table 3. Molecular Weight Characteristic of (Co)polymers

			MW	
run	catalyst system	sample	M_w (Kg mol^{-1})	MWD
1	Cat-A	PE-I-nPS	290	3.5
2		PEH70-I-nPS	201	2.3
3		PEH150-I-nPS	180	3.0
4	Cat-B	PE-I-SiO_2	1760	9.5
5		PEH70-I-SiO_2	n.d.	n.d.
6		PEH150-I-SiO_2	690	11.2
7	Cat-C	PE-BI-nPS	552	3.4
8		PEH70-BI-nPS	251	3.3
9		PEH150-BI-nPS	133	2.3
10	Cat-D	PE-BI-SiO_2	590	5.0
11		PEH70-BI-SiO_2	377	3.6
12		PEH150-BI-SiO_2	162	3.3

MWs for the polymers produced by silica-supported metallocenes are higher than their nPS-supported counterparts. However, in the corresponding copolymerizations, the MW of copolymers drops (Table 3). The MW of the copolymers provided by Cat-A, using organic supports, diminishes the least (from 290 to 180 Kg mol^{-1}). Generally, this decrease in the average MW of all copolymers by reducing the high MW fractions (Figure 5) suggests simple chain termination reactions, for example, chain transfer to the comonomer or β-H-elimination.[8] Therefore, this demonstrates that the softer nature of the nPS supports retains the MW of the product closer to the amount made with identical homogeneous metallocenes (145 Kg mol^{-1} for **I** catalyst[31]).

In addition to MW, the MWD of the polymers was altered by the type of the support. Compared to the MWD reported for the polymers produced with metallocenes in solution/homogeneous polymerization (MWD < 2[32]), using support broadens the MWD of the PE products.[33,34] The MWD of the polymers produced by Cat-A and Cat-C is only slightly increased (MWD = 2 to 3.5) using the metallocenes (**I** and **BI**) on organic supports. However, the increase in distribution is much more pronounced for (co)polymers derived from both silica-supported metallocenes (Figure 5, runs 4−6 and 10−12 in Table 3).

On the one hand, immobilizing single-site catalysts on the support restrict the spatial access of monomers to the catalytic centers. On the other hand, the hard nature of silica supports imposes diffusion barriers to reach inner active centers by producing a crystalline PE layer around the particles in the instance of the polymerization (filter effect). In contrast, the polymeric PEG chains are more flexible to keep the catalytic centers accessible to monomers and avoid broadening in the MWD.

Another possible explanation is that the aluminum is distributed on both supports differently. Similar to the discussion in section 3.1, in the case of nPS supports, Al, and consequently, the active centers are distributed on the surface as well as inside of the support aggregates. Because of the soft organic material, which can uptake the monomers more conveniently, no diffusion barriers hamper the monomer access to the inner catalyst sites. However, for SiO_2-supported catalysts, Al is distributed mostly on (or close to) the surface of the support, and especially when the polymerization kinetic is slow, monomers are faced with mass transfer and penetration issues to reach interior active centers.

For the catalyst structure role, the MWD of the polymers produced by Cat-B is broader than that of the corresponding (co)polymers of Cat-D. The influence of the support in controlling the MW for the **BI** catalyst on both supports is less than catalyst **I**. The potential explanation is the higher activity of the **BI** catalyst compared to the **I** catalyst. The more active the catalyst is, the faster fragmentation and accessibility to the

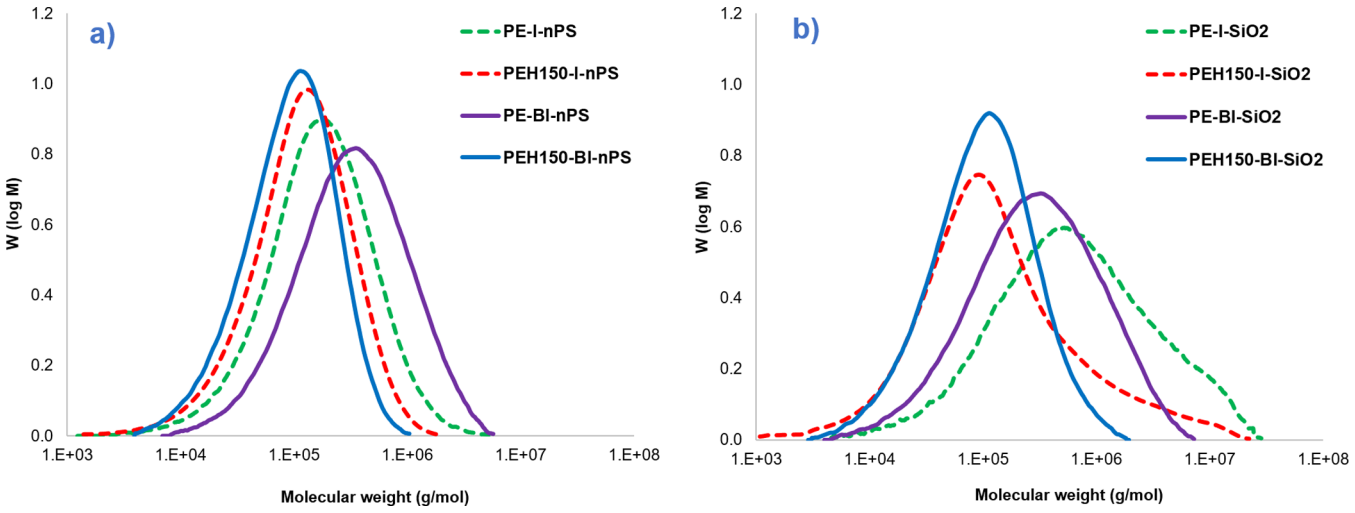

Figure 5. Effect of catalyst and support modes on the MW distributions of the as-synthesized homo- and copolymers (a) nPS support and (b) SiO_2 support.

https://dx.doi.org/10.1021/acs.macromol.0c01920
Macromolecules 2021, 54, 2667−2680

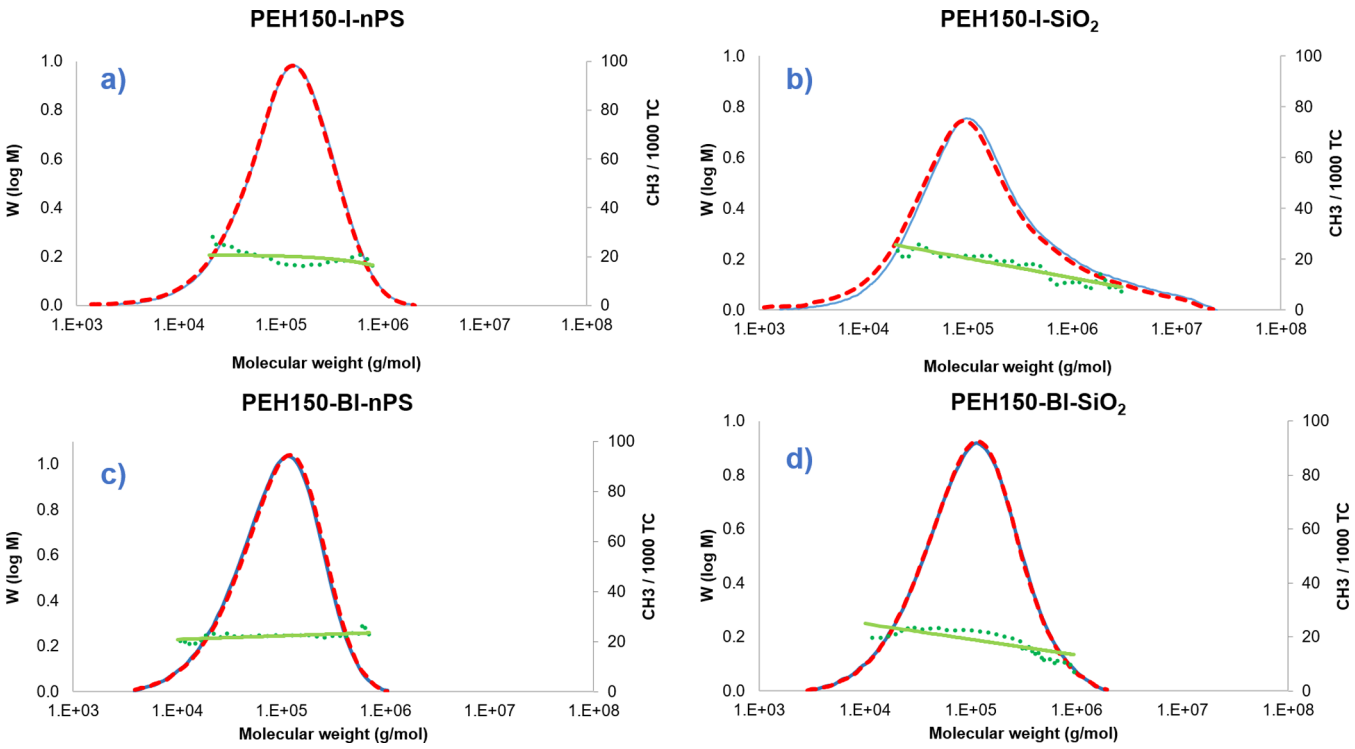

Figure 6. Comonomer distribution in different MW fractions depending on the support type.

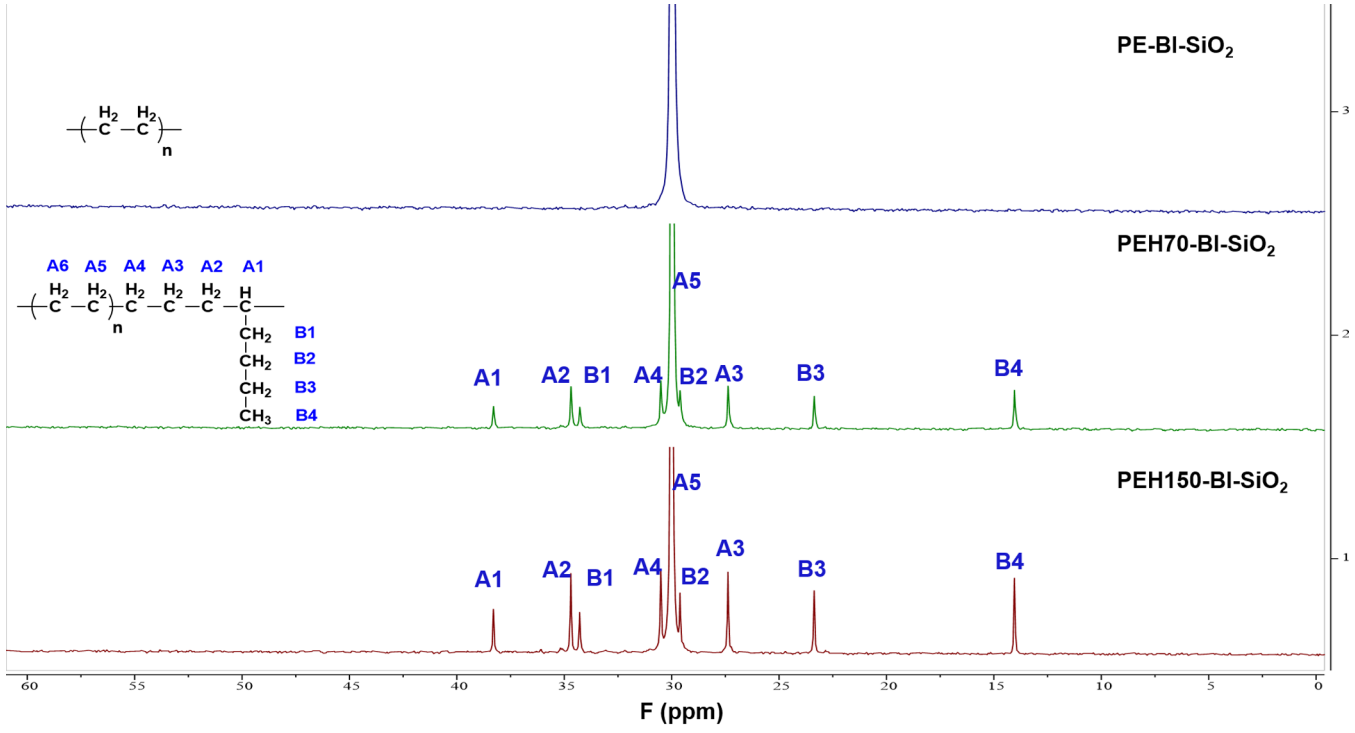

Figure 7. ^{13}C NMR spectra of PEs prepared by Cat-D.

inner active centers can occur. However, the possibility of producing polymers with a broad MW distribution employing metallocene catalysts might sometimes be interesting for special applications.[8,35,36,37]

3.3.2. Study on Branching and Branch Distribution. Short-chain branches, here butyl branches, are introduced by the insertion of the comonomer 1-hexene into the polymer chains. The number of SCB per 1000 backbone carbon atoms (SCB) and its distribution (SCBD) within the polymer chain are two microstructural parameters influencing the long-term performance of polyethylene, for example, stress-crack resistance.[38] Therefore, the design of catalyst systems that regulate the fine tuning of the polymer microstructure is particularly desirable in this context. Following the MW and MWD studies, a possible correlation between the type of the support and polymer structure was explored. The focus was mainly on the polymer

https://dx.doi.org/10.1021/acs.macromol.0c01920
Macromolecules 2021, 54, 2667−2680

Table 4. Chemical Composition of (Co)polymers

			SSA			NMR	
run	catalyst system	sample	SCB (/1000 C)	C_6 (mol %)	SCBD	SCB (/1000 C)	C_6 (mol %)
1	Cat-A	PE-I-nPS	0.0	0.0		0.0	0.0
2		PEH70-I-nPS	11.0	2.3	1.20	14.0	3.0
3		PEH150-I-nPS	16.0	3.4	1.10	20.0	4.2
4	Cat-B	PE-I-SiO_2	0.0	0.0		0.0	0.0
5		PEH70-I-SiO_2	13.0	2.7	2.20	15.0	3.3
6		PEH150-I-SiO_2	12.0	2.5	2.80	14.0	3.0
7	Cat-C	PE-BI-nPS	0.0	0.0		0.0	0.0
8		PEH70-BI-nPS	18.4	4.0	1.07	20.8	4.6
9		PEH150-BI-nPS	21.7	4.8	1.05	24.8	5.5
10	Cat-D	PE-BI-SiO_2	0.0	0.0		0.0	0.0
11		PEH70-BI-SiO_2	16.3	3.5	1.40	13.6	2.9
12		PEH150-BI-SiO_2	18.8	4.1	1.80	16.7	3.6

CCD aspect, including the number and distribution of branching. The CCD provides information regarding the intramolecular and intermolecular comonomer distribution. NMR spectroscopy, DSC endotherms using the SSA technique, and GPC-IR were used for quantitative and qualitative analyses.

3.4. GPC-IR Spectroscopy Correlation. The influence of the soft organic support was investigated as a responsible factor for the comonomer distribution in the PE chains. To confirm this, the dependence of the comonomer distribution with the MWs of the polymers was visualized by IR detection in GPC experiments [see Figures 6 and S6 (Supporting Information)]. The number of branching measured by this method is overestimated because of the ethylene/1-octene calibration curve available for the IR detector, which is not precisely for ethylene/1-hexene. Therefore, this approach is used only for following the chemical composition qualitatively.

The butyl branches are distributed homogenously over different MWs for copolymers made by both catalysts supported on nPS (Figure 6a,c) and heterogeneously for copolymers made by silica-supported catalysts (Figure 6b,d). In particular, for the samples prepared by both Cat-B (**I** on SiO_2) and Cat-D (**BI** on SiO_2), the comonomer is mostly inserted in the chains with lower MW, which is in line with the observations from the filter effect.[21] Accordingly, the rigidity of a support and how freely monomers can reach the catalytic center are crucial factors in regulating the insertion of the comonomer to the growing chain.

3.5. NMR Spectroscopy. ^{13}C NMR spectroscopy is used to analyze the microstructure of (co)polymers. In the obtained copolymers, some characteristic peaks are detected because of the formation of short-chain (butyl) branches by the comonomer incorporation. The corresponding spectra are a proof of incorporating the comonomer into the polymer chains (Figure 7). All signals corresponding to the main chain and branching are indicated with A (main chain) and B (branching), respectively (see the other spectra in Supporting Information, Figure S8). There is no signal related to the branching for the homopolymerization condition of ethylene (runs 1, 4, 7, and 10) for all four catalyst systems as expected to produce high-density polyethylene. The signals related to branches are more pronounced as a function of the comonomer concentration in the polymerization feed. The characteristic signals in ^{13}C NMR spectra for copolymer samples using all four catalyst systems, on both supports (Figure 7, runs 2−3, 5−6, 7−9, and 11−12 in Table 4), demonstrate a high number of branching.

The branching content is estimated from the ^{13}C NMR spectra of the polymers using established procedures[39] based on the Randall method (results in Table 4). Cat-C and then Cat-A give the highest number of branching in the polymer chains. These numbers increase as a function of comonomer concentration in the polymerization reaction (21−25 and 14−20 branches per 1000 C atom, respectively). In comparison, both Cat-D and Cat-B incorporate 14−17 branching/1000 carbon atoms using identical conditions. For the latter, a small increase in the SCBs is observed similar to earlier reports,[4,29] as 1-hexene concentration increases in the copolymerization feed.

In the case of the catalyst structure in ethylene/1-hexene copolymerization (Table 4), benzannelation of the indenyl ligand increases the molar content of 1-hexene in the polymer (runs 2−3, 4−6 *vs* 8−9, 11−12). This confirms the earlier findings by Mülhaupt et al. for ethylene/1-octene copolymerization with homogeneous metallocenes.[31]

3.6. DSC−SSA Studies. As a central hypothesis in this study, the influence of the support type on the SCBD along the polymer chains is also investigated using the successive self-nucleation annealing performed using the DSC (SSA−DSC) technique. As a result of comonomer insertion in PE chains, SCB disturbs the polymer crystallization process.[40] The thermal fractionation of copolymers by the SSA is based on the principle that the crystal lamellae thickness is correlated to the length of a successive methylene sequence,[40−42] based on the polyolefins microstructure, SCB, and SCBD. In particular, the number of SCB and SCBD along the polymer chains directly stimulates the formation of crystal units with different lamella lengths. As a result, depending on the SCBD, the final polymer bears different crystal units with different lamellar thicknesses (with corresponding melting temperatures—additional information can be found in the Supporting Information).

Notably, it is already established that the pure PE sample shows only one DSC peak.[40] However, for the copolymer samples, the signal areas distributed along the temperature axis represent the melting of the lamella formed by molecules having similar content and distribution of SCB. In the opposite of the segments with negligible branching, the lowest T_m represents segments in which the regularity of methylene sequences is abrogated by the highest number of SCB; thus, crystallization is hindered.[43] In addition to the observed dependency of SCBD by the support type visualized by GPC-

https://dx.doi.org/10.1021/acs.macromol.0c01920
Macromolecules 2021, 54, 2667−2680

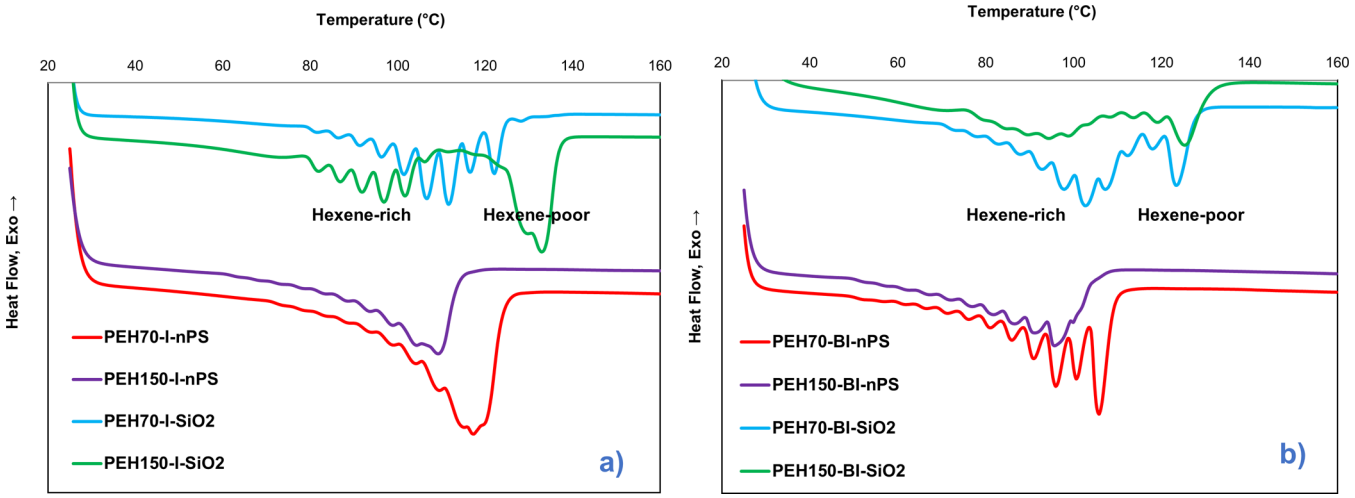

Figure 8. DSC heating scans at 10 °C min^{-1} after SSA thermal treatment fractionation for PE copolymers produced by (a) **I** and (b) **BI** catalysts on inorganic and organic supports.

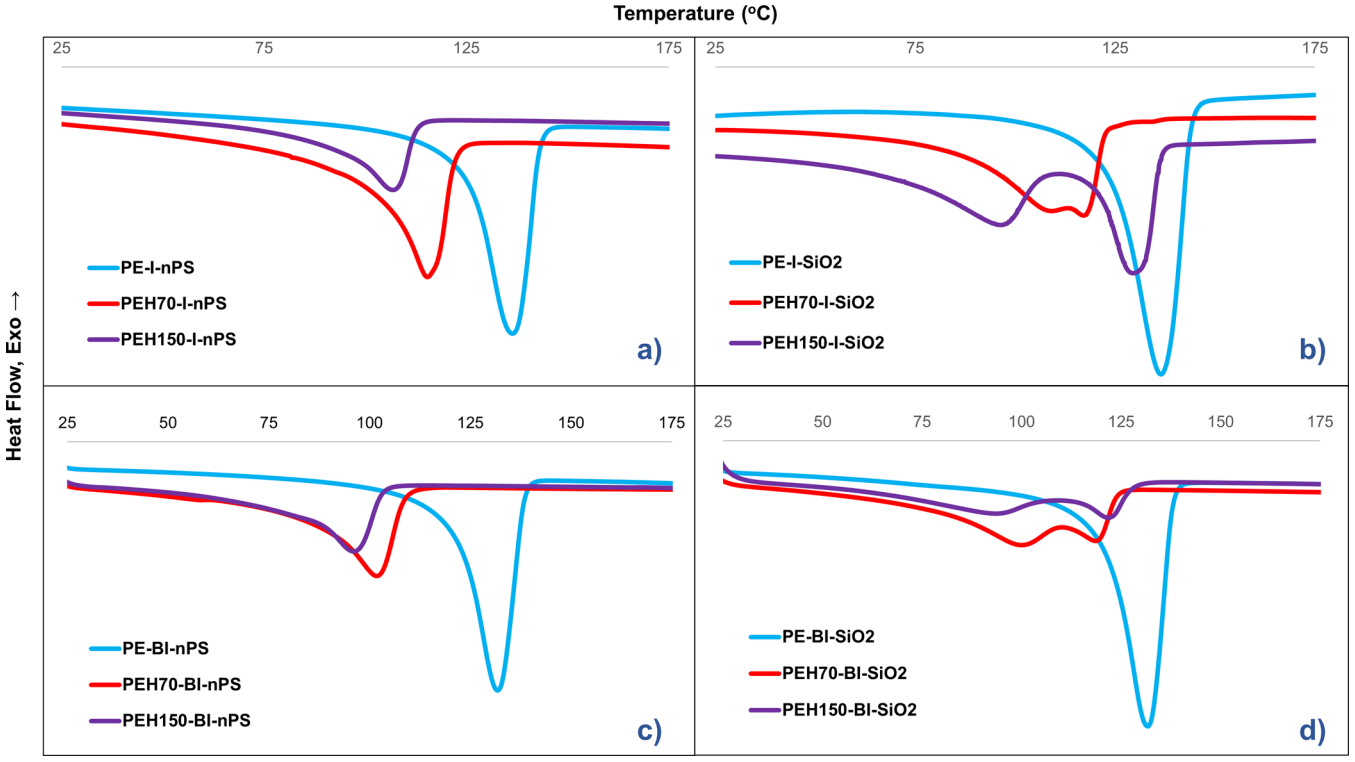

Figure 9. Melting behavior of the produced polymers.

IR and NMR spectroscopy, copolymer samples were studied using the SSA technique.

The corresponding SSA curves of the copolymers are presented in Figure 8. The more uniform lamellar populations are, the more homogeneously the branches are distributed along the polymer chains (narrow branching dispersity, SCBD≈1, see Supporting Information).

The support type plays a primary role in the shape of the SSA thermal curves. Figure 8 shows that the melting peaks of different lamellar populations are spread more uniformly for resultant copolymers from Cat-A to Cat-C. In the silica case, however, peaks are distributed nonuniformly along the temperature axis for Cat-B and Cat-D copolymers. This nonuniformity represents comonomer-rich and comonomer-poor segments within a PE chain (pointed in Figure 8). They become more discrete as a function of the comonomer concentration in the feed. Accordingly, the corresponding SCBD contents (Table 4) range from about 1.1 (for nPS-supported catalysts, runs 2, 3, 8, and 9) to over 2 (for silica-supported catalysts, runs 5, 6, 11, and 12), which confirm the result of GPC-IR analysis. Such heterogeneities in the CCD of the copolymers are attributed to the different fragmentation behavior of silica supports (layer-by-layer) *versus* nPS (multi-grain) supports because of the rigid or soft nature of these supports, respectively.

Consequently, the shape of SSA curves is dependent on the chemical composition and the number of branches in the copolymers. Similar to NMR results, a high number of peaks

https://dx.doi.org/10.1021/acs.macromol.0c01920
Macromolecules 2021, 54, 2667−2680

Table 5. Thermal and Crystallinity Properties of the (Co)polymers Prepared by Catalyst Systems Cat-A to Cat-D

			thermal properties			XRD
run	catalyst system	sample	T_m (°C)	T_c (°C)	X_c (%)	X_c (%)
1	Cat-A	PE-I-nPS	135.7	114.0	56.8	58.7
2		PEH70-I-nPS	114.7	98.3	37.1	42.5
3		PEH150-I-nPS	106.2	88.0	30.8	35.2
4	Cat-B	PE-I-SiO_2	136.2	115.6	35.8	35.9
5		PEH70-I-SiO_2	111.3[a] (109.2, 117)	96.0[a] (65.2, 102.9)	22.6	29.6
6		PEH150-I-SiO_2	113.2[a] (96, 129.6)	94.8[a] (58.4, 84.4, 116.7)	19.3	27.3
7	Cat-C	PE-BI-nPS	131.9	117.4	50.0	44.5
8		PEH70-BI-nPS	101.9	87.7	25.6	27.5
9		PEH150-BI-nPS	96.3	79.1	20.2	23.3
10	Cat-D	PE-BI-SiO_2	131.8	116.2	42.2	37.3
11		PEH70-BI-SiO_2	105.5[a] (118.7, 100.2)	89.2[a] (124.9,103.4)	15.1	24.4
12		PEH150-BI-SiO_2	101.3[a] (121.8, 93.6)	84.2[a] (103.1, 74.3)	13.8	20.0

[a]These data are calculated based on the number average of peaks: $\bar{X} = \frac{\sum X_i A_i}{\sum A_i}$, where X can be T_m or T_C and A is the integral enthalpy of every peak.

for the copolymers prepared with Cat-A to Cat-D (Figure 8) indicate high comonomer incorporation.

The relationship between the observed melting temperature (T_m) and the content of SCB has been quantified by the Hosoda equation.[41] Moreover, the comonomer content in the polymer chain is calculated based on available equations (results in Table 4, see Supporting Information).

By comparing the data (Table 4), similar trends to the NMR results have been observed. Because of the higher flexibility to reconfigure, the organic supported catalysts (Cat-A and Cat-C) provide more spatial room for comonomers to coordinate and incorporate a higher number of SCBs (about 25%).

To sum up, all the three methods, that is, GPC-IR spectroscopy, ^{13}C NMR spectroscopy, and SSA, which are used to study the branching distribution, confirm the assumption that the nature of the support has a crucial effect on the copolymerization using heterogeneous catalyst systems. To reach the active sites, the monomer(s) have to diffuse through the porous structure of the supported catalysts in the early polymerization stages and then through the polymer layer surrounding the active sites once polymerization begins, which might impede the ongoing comonomer incorporation.[11,16] When intraparticle diffusion is rapid with respect to the polymerization rate, the effect of mass-transfer resistance on the CCD is negligible (Cat-A and Cat-C). However, if comonomer penetration is slow, this will affect the molecular properties of polyethylene, for example, MWD (see section 3.3.1) and CCD (see this section). Therefore, a balance between catalyst activity and fragmentation behavior (both correlated to the support type) determines the monomer diffusion behavior to the active centers.

3.7. Bulk Properties. Polymer composition studies (section 3.3) confirmed the central hypothesis about the controlling influence of the type of the support on the resulting polymer microstructures. In direct association, the bulk properties of a polymer, such as average crystallinity and melting behavior, are the most critical for processing and application.

3.8. Melting Temperature. The role of supporting metallocenes using different comonomer concentrations in the polymerization in the melting and crystallization behavior is investigated by DSC. The melting temperature (T_m) can be one of many indicators of SCB in PE. The T_m values are closely related to the structural characteristics of the polymer crystalline phase. Figure 9 shows that the average melting peaks are shifted to lower temperatures (Table 5- runs 1−12) as a function of the number of SCBs (for all Cat-A to Cat-D, Table 4).

Following the role of the support type, copolymers synthesized with **I** and **BI** catalysts on nPS (Cat-A and Cat-C) show only one melting peak. Thus, the average T_m value drops from 136 to 110 °C and 132 to 96 °C, respectively (Table 5, runs 1−3 and 7−9), to form LLDPE under similar polymerization conditions. In contrast to those systems, for copolymers obtained from **I** and **BI** catalysts on SiO_2 (Cat-B and Cat-D), the additional peaks appear in the higher temperature region as further proof of the inconsistency in comonomer insertion, as already shown by SSA and GPC-IR. This behavior is repeated for both catalysts and both comonomer concentrations [70 (runs 5 and 11) and 150 mmol L^{-1} (runs 6 and 12)]. These two peaks get more discrete by increasing the comonomer concentration in the reactor (Figure 9). In other words, the more comonomer concentration applies a higher diffusional competition between monomers.

The appearance of a double melting peak in the DSC curves obtained from the copolymers can be explained by the so-called "filter-effect" theory.[21] Fink et al. attributed the CCD of ethylene/1-hexene copolymers prepared with a SiO_2/MAO/metallocene system to mass-transfer resistance. They demonstrated that the crystalline layer of the PE polymer wrapping the silica-supported metallocene particle is rapidly formed in the early reaction moments. It progresses after a slow fragmentation, as shown in Supporting Information, via a gradually layer-by-layer fragmentation from the surface up to the center because of the hydraulic forces. It imposes the mass diffusional barrier, which differs the permeability of ethylene and 1-hexene. Henceforward, this filter effect leads to a polymer particle comprising an ethylene-rich center and an enveloped layer formed by the hexene-rich copolymer. Thus, this results in a broad overall CCD, even when copolymerized with metallocene catalysts.

As a result, organic supports can control the copolymer's CCD by the soft nature of support because of the more convenient diffusional and swelling behaviors. Easier fragmentation and homogeneous distribution of the active sites of the

https://dx.doi.org/10.1021/acs.macromol.0c01920
Macromolecules 2021, 54, 2667−2680

catalyst when supported on organic nPS dominate this inspired aspect by the inorganic (SiO_2) support.

3.9. Crystallinity. The crystallinity percentage (X_c) of the final polymer products, significant for mechanical properties, for example, tensile strength,[44] is measured by DSC and wide-angle XRD (Table 5).

The X_c values (provided from DSC) of the homopolymers resulting from Cat-A to Cat-D are between 57 and 36%. By copolymerization, the X_c value is reduced to less than 14%, associated with the SCB contents. To highlight the impact of the support, as it was mentioned before, metallocenes immobilized on organic supports introduced a higher number of SCBs into the polymer chains. Nonetheless, the crystallinity of the corresponding copolymers is higher (57−31% in runs 1−3 and 50−20% in runs 7−9) than the corresponding copolymers from silica-supported metallocenes (36−19% in runs 4−6 and 42−14% in runs 10−12). These results can be taken into account for lowering the chain regularity because of intramolecular heterogeneity in the polymer microstructure. The lower crystallinity in runs 4 and 10 compared to runs 1 and 7 reveals heterogeneity in the different growing chains, which is induced by the hard nature of silica and nonuniform distribution of active centers (Al distribution in Figure 3) even in the absence of comonomers. This phenomenon is more apparent in copolymers with double melting and crystallization temperatures, resulting from the formation of two inconsistent lamellar populations from hexene-poor and hexene-rich fractions.

Besides DSC studies, the crystallinity of the yielded polymers was measured by XRD. The results (Table 5) show results and trends similar to the calorimetry method. The difference between the two measurements becomes more distinguished when there is heterogeneity in the CCD of the polymers (runs 4−6 and 10−12). For instance, the inconsistency revealed as double melting peaks in DSC is not distinguishable by the shape of the peaks or the average calculated X_c preserved by XRD.

4. SUMMARY

The copolymerization of ethylene/1-hexene with supported metallocenes is investigated. The differences in the MW, MWD, SCB, and X_c of the obtained copolymers indicate that the diffusion process of the monomers plays a decisive role in the comonomer incorporation. All measurements together verify the strong impact of the type of support, which is, silica and aggregated nPS particles, on the control of the final copolymer microstructure. The rigid nature of silica results in a heterogeneous distribution of the active sites. Thus, polymerization occurs dominantly on the surface of the unfragmented silica particles, yielding a crystalline polymer shell. This layer affects the diffusion of the monomers, in particular for 1-hexene, because of their bigger size. This filter effect causes a locally different monomer/comonomer concentration at the catalytic centers on the surface and inside the silica pores. Consequently, broadening in MWD and CCD is observed.

In contrast, using organic supports, this broadening is suppressed. It is concluded that the filtering effect is negligible, as the soft organic support has a higher affinity to the nonpolar monomers, which facilitates their uptake and is independent of monomer size in the secondary particles. Therefore, the monomer ratio is similar at all catalytic sites. The polymerization takes place not only on the surface but also inside the support from the beginning on. For both metallocenes, the organic nPS support could compensate for the inhomogeneous comonomer incorporation to synthesize more uniform microstructured copolymers.

5. CONCLUSIONS

The properties of polyolefins obtained with metallocene-catalyzed polymerizations are typically modified by varying catalysts and polymerization parameters. However, the support is considered as an inert compound during the polymerization process, as inorganic supports have been mainly focused on. This study proves that altering the support from inorganic to organic provides a dramatic control over the product properties during the polymerization process, which is demonstrated by comparing the polymer properties obtained from catalysts that are loaded on different organic and inorganic supports. The experiments show, for metallocene catalysts immobilized on different types of supports, that MW, MWD, and CCD of copolymers can be altered. Various comonomers such as 1-butene, norbornene, or higher α-olefins are applicable to produce different microstructures. Especially in copolymerization, organic supports/MAO/metallocene keep the polymer properties significantly close to the behavior of corresponding single-site catalysts in solution polymerization. Therefore, the organic nPS supports dominate the reported mass-transfer barrier induced by the rigid nature of the SiO_2 support and nonuniform distribution of catalyst active centers. This method generally provides more homogeneous products rather than a mixture of products as produced by supported metallocene on silica or other inorganic supports. Moreover, this approach facilitates the catalyst selection for various desired properties, as, so far, there are only a few reported metallocene catalysts that depict lower nonuniformity in the polymer structure when the catalyst is loaded on the silica particles.

■ ASSOCIATED CONTENT

Supporting Information

The Supporting Information is available free of charge at https://pubs.acs.org/doi/10.1021/acs.macromol.0c01920.

Polymer particle size using optical microscopy, ToF-SIMS, and SEM-EDX of aluminum distribution on the support, GPC measurement method and SCB calculation, ICP-OES sample preparation, crystallinity calculation by XRD, NMR calculations and spectrums, and SSA calculation (PDF)

■ AUTHOR INFORMATION

Corresponding Authors

Hassan Arabi − *Iran Polymer and Petrochemical Institute, Tehran 1497713115, Iran*; Email: h.arabi@ippi.ac.ir

Markus Klapper − *Max Planck Institute for Polymer Research, Mainz 55128, Germany*; orcid.org/0000-0003-2905-2392; Email: klapper@mpip-mainz.mpg.de

Authors

Zahra-Alsadat Hejazi-Dehaghani − *Max Planck Institute for Polymer Research, Mainz 55128, Germany; Iran Polymer and Petrochemical Institute, Tehran 1497713115, Iran*

Daniel Thalheim − *Max Planck Institute for Polymer Research, Mainz 55128, Germany*

Danijel Vidakovic − *Max Planck Institute for Polymer Research, Mainz 55128, Germany*

https://dx.doi.org/10.1021/acs.macromol.0c01920
Macromolecules 2021, 54, 2667−2680

Mehdi Nekoomanesh Haghighi − *Iran Polymer and Petrochemical Institute, Tehran 1497713115, Iran*
Lothar Veith − *Max Planck Institute for Polymer Research, Mainz 55128, Germany*

Complete contact information is available at: https://pubs.acs.org/10.1021/acs.macromol.0c01920

Notes

The authors declare no competing financial interest.

■ ACKNOWLEDGMENTS

The authors are grateful to Dr. Manfred Wagner for the NMR experiments of ethylene copolymers and Dr. Jan-Hendrik Arndt and Dr. Ali Safinejad for valuable assistance with the GPC measurements. Many thanks go to Eva Deister for the DSC and SSA experiments.

■ REFERENCES

(1) Matsko, M. A.; Echevskaya, L. G.; Vanina, M. P.; Nikolaeva, M. I.; Mikenas, T. B.; Zakharov, V. A. Study of the compositional heterogeneity of ethylene/1-hexene copolymers produced over supported catalysts of different composition. *J. Appl. Polym. Sci.* **2012**, *126*, 2017−2023.
(2) Francesco, Z.; Cipullo, R.; Busico, V.; Ehm, C. Separating Electronic from Steric Effects in Ethene/α-Olefin Copolymerization: A Case Study on Octahedral [ONNO] Zr-Catalysts. *Processes* **2019**, *7*, 384.
(3) Kaminsky, W. The discovery and evolution of metallocene-based olefin polymerization catalysts. *Rendiconti Lincei. Sci. Fis. Nat.* **2017**, *28*, 87−95.
(4) Yang, G.; Meng, L.; Che, A.; Huang, Y.; Li, R. High performance gas-phase ethylene polymerization metallocene catalyst investigation in a pilot-plant fluidized bed reactor (1) experimental analysis. *Powder Technol.* **2018**, *327*, 310−319.
(5) Naundorf, C.; Matsui, S.; Saito, J.; Fujita, T.; Klapper, M.; Müllen, K. Ultrahigh molecular weight polyethylene produced by a bis(phenoxy-imine) titanium complex supported on latex particles. *J. Polym. Sci., Part A: Polym. Chem.* **2006**, *44*, 3103−3113.
(6) Nenov, S.; Clark, C. G.; Klapper, M.; Müllen, K. Metallocene-catalyzed polymerization in nonaqueous fluorous emulsion. *Macromol. Chem. Phys.* **2007**, *208*, 1362−1369.
(7) Choi, Y.; Soares, J. B. P. Supported single-site catalysts for slurry and gas-phase olefin polymerisation. *Can. J. Chem. Eng.* **2012**, *90*, 646−671.
(8) Paulik, C.; Spiegel, G.; Jeremic, D. Bimodal Polyethylene: Controlling Polymer Properties by Molecular Design. *Multimodal Polymers with Supported Catalysts*; Springer International Publishing, 2019: pp 243−265.
(9) Saadat, S.; Soares, J. B. P.; Deslauriers, P. J.; Fodor, J. S. Polymerization Kinetics and Microstructure of Ethylene/1-Hexene Copolymers Made with Dual Metallocenes. *Macromol. React. Eng.* **2020**, *14*, 1900032.
(10) Klapper, M.; Joe, D.; Nietzel, S.; Krumpfer, J. W.; Müllen, K. Olefin polymerization with supported catalysts as an exercise in nanotechnology. *Chem. Mater.* **2014**, *26*, 802−819.
(11) Ahsan Bashir, M.; McKenna, T. F. L. Reaction Engineering of Polyolefins: The Role of Catalyst Supports in Ethylene Polymerization on Metallocene Catalysts. In *Polymer Reaction Engineering of Dispersed Systems*; Pauer, W., Ed.; Springer International Publishing: Cham, 2017: pp 19−63.
(12) Brentano, L.; Martins, C.; Borba, M. Hybrid silica based catalysts prepared by the encapsulation of zirconocene compound via non-hydrolytic sol-gel method for ethylene polymerization. *Appl. Catal., A* **2018**, *560*, 225−235.
(13) Velthoen, M. E. Z.; Boereboom, J. M.; Bulo, R. E.; Weckhuysen, B. M. Insights into the activation of silica-supported metallocene olefin polymerization catalysts by methylaluminoxane. *Catal. Today* **2019**, *334*, 223−230.
(14) Heurtefeu, B.; Bouilhac, C.; Cloutet, É.; Taton, D.; Deffieux, A.; Cramail, H. Polymer support of "single-site" catalysts for heterogeneous olefin polymerization. *Prog. Polym. Sci.* **2011**, *36*, 89−126.
(15) Velthoen, M. E. Z.; Muñoz-Murillo, A.; Diefenbach, S.; Weckhuysen, B. M. The Multifaceted Role of Methylaluminoxane in Metallocene-Based Olefin Polymerization Catalysis. *Macromolecules* **2018**, *51*, 343−355.
(16) Bashir, M. A.; Monteil, V.; Boisson, C.; Mckenna, T. F. L. Experimental Proof of the Existence of Mass-Transfer Resistance During Early Stages of Ethylene Polymerization with Silica Supported Metallocene/MAO Catalysts. *AIChE J.* **2017**, *63*, 4476.
(17) Jamnongphol, S.; Jaturapiree, A.; Sukrat, K.; Saowapark, T.; Chaichana, E.; Jongsomjit, B. Rice Husk-Derived Silica as a Support for Zirconocene/MMAO Catalyst in Ethylene Polymerization. *Waste Biomass Valorization* **2020**, *11*, 769−779.
(18) Jang, Y.-J.; Naundorf, C.; Klapper, M.; Müllen, K. Study of the fragmentation process of different supports for metallocenes by laser scanning confocal fluorescence microscopy (LSCFM). *Macromol. Chem. Phys.* **2005**, *206*, 2027−2037.
(19) Nietzel, S.; Joe, D.; Krumpfer, J. W.; et al. Organic Nanoparticles as Fragmentable support for Ziegler-Natta catalysts. *J. Polym. Sci., Part A: Polym. Chem.* **2015**, *53*, 15.
(20) Freudensprung, I.; Joe, D.; Nietzel, S.; Vollmer, D.; Klapper, M.; Müllen, K. Spherical Polyolefin Particles from Olefin Polymerization in the Confined Geometry of Porous Hollow Silica Particles. *Macromol. Rapid Commun.* **2016**, *37*, 1651−1656.
(21) Przybyla, C.; Tesche, B.; Fink, G. Ethylene/hexene copolymerization with the heterogeneous catalyst system SiO2/MAO/rac-Me2Si[2-Me-4-Ph-Ind]2ZrCl2: The filter effect. *Macromol. Rapid Commun.* **1999**, *20*, 328−332.
(22) Naundorf, C.; Ferrari, D.; Rojas, G.; Fink, G.; Klapper, M.; Müllen, K. Hard versus Soft Materials as Supports for Metallocene and Post-Metallocene Catalysts. *Macromol. React. Eng.* **2009**, *3*, 456−466.
(23) Wang, X.; Han, X.; Ren, F.; Xu, R.; Bai, Y. Porous Organic Polymers-Supported Metallocene Catalysts for Ethylene/1-Hexene Copolymerization. *Catalysts* **2018**, *8*, 146.
(24) Koch, M.; Stork, M.; Klapper, M.; Müllen, K.; Gregorius, H. Immobilization of metallocenes through noncovalent bonding via MAO to a reversibly cross-linked polystyrene. *Macromolecules* **2000**, *33*, 7713−7717.
(25) Quijada, R.; Dupont, J.; Miranda, M. S. L.; Scipioni, R. B.; Galland, G. B. Copolymerization of ethylene with 1-hexene and 1-octene: correlation between type of catalyst and comonomer incorporated. *Macromol. Chem. Phys.* **1995**, *196*, 3991−4000.
(26) Campos, J. M.; Lourenço, J. P.; Cramail, H.; Ribeiro, M. R. Nanostructured silica materials in olefin polymerisation: From catalytic behaviour to polymer characteristics. *Prog. Polym. Sci.* **2012**, *37*, 1764−1804.
(27) Kaminsky, W. Production of polyolefins by metallocene catalysts and their recycling by pyrolysis. *Macromol. Symp.* **2016**, *360*, 10−22.
(28) Kaminsky, W.; Fernandes, M. Discovery and development of metallocene-based polyolefins with special properties. *Polyolefins J.* **2015**, *2*, 1−16.
(29) Yang, Q.; Jensen, M. D.; McDaniel, M. P. Alternative view of long chain branch formation by metallocene catalysts. *Macromolecules* **2010**, *43*, 8836−8852.
(30) Jensen, M. D.; Yang, Q.; Yu, Y.; Mcdaniel, M. P. Kinetics of Long-Chain Branch Formation in Polyethylene. *ACS Catal.* **2018**, *8*, 725−737.
(31) Suhm, J.; Schneider, M. J.; Mülhaupt, R. Influence of metallocene structures on ethene copolymerization with 1-butene and 1-octene. *J. Mol. Catal. A: Chem.* **1998**, *128*, 215−227.
(32) Schneider, M. J.; Suhm, J.; Mülhaupt, R.; Prosenc, M.-H.; Brintzinger, H.-H. Influence of Indenyl Ligand Substitution Pattern

on Metallocene-Catalyzed Ethene Copolymerization with 1-Octene. *Macromolecules* **1997**, *30*, 3164−3168.
(33) Brambilla, R.; Radtke, C.; Stedile, F. C.; Dos Santos, J. H. Z.; Miranda, M. S. L. Metallocene catalyst supported on silica-magnesia xerogels for ethylene polymerization. *Appl. Catal., A* **2010**, *382*, 106−114.
(34) Barrera, E. G.; Stedile, F. C.; Brambilla, R.; dos Santos, J. H. Z. Broadening molecular weight polyethylene distribution by tailoring the silica surface environment on supported metallocenes. *Appl. Surf. Sci.* **2017**, *393*, 357−363.
(35) Jayaratne, K. C.; Cymbaluk, T. H.; Jensen, M. D. A Career in Catalysis: Max McDaniel. *ACS Catal.* **2018**, *8*, 602−614.
(36) Romina, A.; Floran, A.; Jeremic, D. *Multimodal Polymers with Supported Catalysts*; Springer, 2019.
(37) Yang, Q.; Greco, J. F.; McDaniel, M. P.; Yu, Y.; Glass, G. L.; Crain, T. R. Dual catalyst systems for producing polymers with a broad molecular weight distribution and a uniform short chain branch distribution. BR 112016027380 A2, 2018.
(38) Sauter, D. W.; Taoufik, M.; Boisson, C. Polyolefins, a success story. *Polymers* **2017**, *9*, 185.
(39) Alkhazaal, A. *Characterization of Ethylene/α-Olefin Copolymers Made with a Single-Site Catalyst Using Crystallization Elution Fractionation*; University of Waterloo, 2011.
(40) Müller, A. J.; Michell, R. M.; Pérez, R. A.; Lorenzo, A. T. Successive self-nucleation and annealing (SSA): correct design of thermal protocol and applications. *Eur. Polym. J.* **2015**, *65*, 132−154.
(41) Matsko, M. A.; Vanina, M. P.; Echevskaya, L. G.; Zakharov, V. A. Study of the compositional heterogeneity of ethylene-hexene-1 copolymers by thermal fractionation technique by means of differential scanning calorimetry. *J. Therm. Anal. Calorim.* **2013**, *113*, 923−932.
(42) Yu, Y.; Mckenna, T. F. L.; Boisson, C.; Miranda, M. S. L.; Martins, O. Engineering Poly(ethylene- co -1-butene) through Modulating the Active Species by Alkylaluminum. *ACS Catal.* **2020**, *10*, 7216−7229.
(43) Białek, M.; Czaja, K.; Sacher-Majewska, B. Studies of structural composition distribution heterogeneity in ethylene/1-hexene copolymers using thermal fractionation technique (SSA): Effect of catalyst structure. *Thermochim. Acta* **2005**, *429*, 149−154.
(44) De Rosa, C.; Ruiz De Ballesteros, O.; Auriemma, F.; et al. Polymorphic behavior and mechanical properties of isotactic 1-butene-ethylene copolymers from metallocene catalysts. *Macromolecules* **2014**, *47*, 4317−4329.

https://dx.doi.org/10.1021/acs.macromol.0c01920
Macromolecules 2021, 54, 2667−2680